

# Cracking behavior of RC shear walls subject to cyclic loadings

Hyo-Gyoung Kwak<sup>†</sup> and Do-Yeon Kim<sup>‡</sup>

*Department of Civil and Environmental Engineering, KAIST,  
373-1 Guseong-dong, Yuseong-gu, Daejeon 305-701, South Korea*

*(Received August 6, 2003, Accepted October 9, 2003)*

**Abstract.** This paper presents a numerical model for simulating the nonlinear response of reinforced concrete (RC) shear walls subject to cyclic loadings. The material behavior of cracked concrete is described by an orthotropic constitutive relation with tension-stiffening and compression softening effects defining equivalent uniaxial stress-strain relation in the axes of orthotropy. Especially in making analytical predictions for inelastic behaviors of RC walls under reversed cyclic loading, some influencing factors inducing the material nonlinearities have been considered. A simple hysteretic stress-strain relation of concrete, which crosses the tension-compression region, is defined. Modification of the hysteretic stress-strain relation of steel is also introduced to reflect a pinching effect depending on the shear span ratio and to represent an average stress distribution in a cracked RC element, respectively. To assess the applicability of the constitutive model for RC element, analytical results are compared with idealized shear panel and shear wall test results under monotonic and cyclic shear loadings.

**Keywords:** pinching effect; shear walls; cyclic behavior; average stress-strain; nonlinear analysis.

---

## 1. Introduction

Reinforced concrete (RC) structures in regions of high seismic risk experience many earthquakes and develop inelastic deformations when subjected to strong earthquakes. Since the inelastic deformations accompany a lot of complex structural behavior, to insure adequate deformation capacity at a given shear stress level, it is usually necessary to determine design parameters affecting strength and deformation capacities in the case of RC shear walls. In order to assess the margin of safety of RC structures against failure, an accurate estimation of the ultimate load is essential and the prediction of the load-deformation behavior of the structure throughout the range of elastic and inelastic response is desirable. Considering these factors, a rigorous nonlinear analysis is required to more exactly evaluate ultimate resisting capacity and load-deformation behavior. Hence, many experimental and analytical studies for predicting the nonlinear behavior according to load reversals and for computing the ultimate resistance of isolated RC shear walls have been performed (CEB 1996, CEB 1996a, Penelis and Kappos 1997).

In contrast, numerical models for FE analyses of RC shear walls, which can provide accurate simulations of cracking behavior under severe loading conditions such as seismic loadings and

---

<sup>†</sup> Associate Professor

<sup>‡</sup> Graduate Student

reversed cyclic loadings, are somewhat less commonly used due to the complexities in the hysteretic modeling of reinforced concrete composite material after cracking or crushing of concrete and yielding of steel.

RC structures representing shear dominant structural behavior show pinched hysteresis responses, which mean poor energy absorption capacities and stiffness degradation as the number of cycles increases. The design procedures for RC shear walls, however, do not take into account these key features of hysteretic response (Sittipunt and Wood 1995). There is no design code that mentions any criterion requested to reserve the ultimate resisting capacity and the corresponding ductility for a RC shear wall subject to cyclic loadings.

The bond mechanism at the reinforcement and surrounding concrete interface plays an important role in reinforced concrete structures. Especially, for shear dominated structures such as panels and shear walls which offer great resistance for lateral loads, concrete cracking, steel yielding and bond slip behavior govern the overall nonlinear response of structures since those structures experience severe strain in the principal tensile direction followed by yielding of steel. Therefore, a numerical model must simulate effectively these nonlinear behavior of structures subjected to in-plane cyclic shear. Based on these aspects, nonlinear FE analysis considering shear deformation effect is definitely required. Moreover, it may be necessary for an enhanced evaluation of hysteretic behavior to model each constituent material and interaction between reinforcing steel and concrete appropriately with complex hysteretic stress-strain relationships.

This paper presents an analytical model for RC shear walls subject to general in-plane loading. The rotating crack assumption is adopted, and simple hysteretic stress-strain curves of concrete and reinforcing steel are introduced. In addition, to consider the shear stiffness degradation visualized as a pinching phenomenon in a hysteretic relation of low-rise shear wall, a direct modification of a hysteretic stress-strain relation of steel is suggested by referring to the existing moment-curvature model which takes into account the pinching effect according to the shear span length (CEB 1996a and Roufaiel and Meyer 1987). The developed numerical model is validated through comparison of the obtained numerical results with experimental data for four idealized orthogonally reinforced concrete shear panels (Vecchio and Collins 1982, Stevens, *et al.* 1991). In addition, to assess the applicability of the material model under different stress conditions, load-deformation relationships obtained are compared with cyclic shear wall test results (Lefas, *et al.* 1990, Oesterle, *et al.* 1976).

## 2. Material model

### 2.1. Concrete

#### 2.1.1. Monotonic envelope

Concrete is assumed to be an orthotropic material in the principal strain directions and is treated as an incremental linear elastic material. The incremental constitutive relationships referring to the principal axes are described as follows:

$$\begin{Bmatrix} d\sigma_{c1} \\ d\sigma_{c2} \\ d\tau_{c12} \end{Bmatrix} = \frac{1}{1-\nu^2} \begin{bmatrix} E_1 & \nu\sqrt{E_1E_2} & 0 \\ \nu\sqrt{E_1E_2} & E_2 & 0 \\ 0 & 0 & (1-\nu^2) \cdot G \end{bmatrix} \begin{Bmatrix} d\varepsilon_1 \\ d\varepsilon_2 \\ d\gamma_{12} \end{Bmatrix} \quad (1)$$

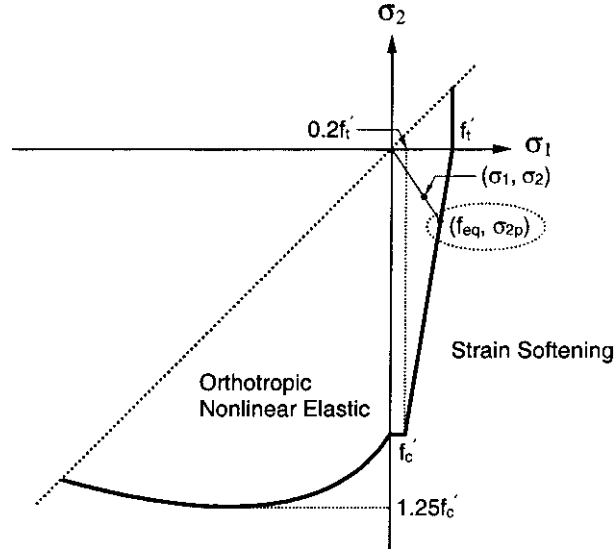


Fig. 1 Biaxial strength failure envelope of concrete

where,  $E_1$  and  $E_2$  are the tangent moduli of the elasticity in the direction of the axes of orthotropy, which are oriented perpendicular and parallel to the crack direction,  $G$  is the secant shear modulus, and  $\nu$  is Poisson's ratio. After cracking, if microcrack zone is fully developed, Poisson's effect disappears.

The most interesting feature of the material stiffness matrix in principal coordinates is the presence of the shear stiffness term, which is implicit to compression field theory due to the assumption that the principal concrete stress direction equals the principal concrete strain direction. This term has the value

$$G = \frac{1}{2} \cdot \frac{\sigma_{c1} - \sigma_{c2}}{\epsilon_1 - \epsilon_2} \quad (2)$$

Most of a wall subjected to shear forces experiences biaxial stress combinations in the tension-compression region. Accordingly, the biaxial strength envelope in the tension-compression region is regarded as of great importance. In this paper, the biaxial strength envelope proposed by Kupfer, *et al.* (1973), shown in Fig. 1, is used, and the accompanying equation for the failure envelope in the tension-compression region is expressed by

$$\frac{\sigma_{1p}}{f'_t} = 1 - 0.8 \frac{\sigma_{2p}}{f'_c} \quad (3)$$

where compressive stresses are assumed to be negative and tensile stresses positive, and the principal stress directions are chosen so that  $\sigma_1 \geq \sigma_2$  algebraically;  $\sigma_{1p}$  and  $\sigma_{2p}$  are the maximum principal stresses corresponding to the current principal stresses  $\sigma_1$  and  $\sigma_2$ , respectively.

As cracks propagate and widen, the concrete struts are disconnected and are finally crushed.

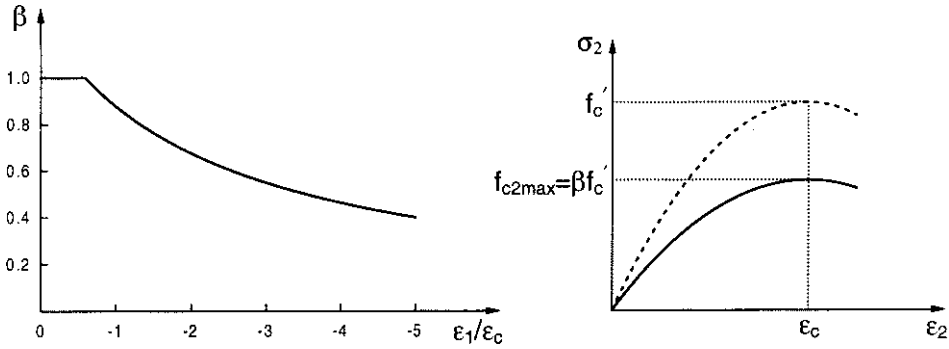


Fig. 2 Strength reduction factor  $\beta$  (Vecchio and Collins 1993)

Accordingly, the compressive strength of concrete decreases due to opening of the cracks. Vecchio, *et al.* (1982) verified this phenomenon clearly through shear panel tests under in-plane loading and showed that the tension cracking reduces the compressive strength in the tension-compression region.

To describe the biaxial behavior of concrete in this region, therefore, the experimental relation proposed by Vecchio, *et al.* (1993) is used in this study. The relation between the compressive strength and the principal tensile strain is defined by the following equation (see Fig. 2).

$$\frac{f_{c2\max}}{f'_c} = \frac{1}{1 + K_c} = \frac{1}{1 + 0.27\left(\frac{\varepsilon_1}{\varepsilon_c} - 0.37\right)} = \beta \leq 1.0 \quad (4)$$

where  $f_{c2\max}$  is the reduced compressive strength,  $\varepsilon_1$  is the principal tensile strain,  $\varepsilon_c$  is the strain corresponding to uniaxial compressive strength, and  $\beta$  is the reduction coefficient.

In describing the uniaxial compressive stress-strain relation of concrete, the model of Thorenfeldt, *et al.*, later calibrated by Collins, *et al.* (Vecchio and Collins 1993) is used. To provide the confinement effect which brings significant increase in ductility, the strain-softening branch in compression for confined concrete is described by a straight line proposed by Kappos (1991). After cracking, tensile stresses in the concrete also arise from interactions between the reinforcement and the concrete. In this study, the tension stiffening relation developed by Kwak and Kim (2001) is adopted to define the envelope curve in the tension softening part. More details for the confinement effect and tension stiffening effect of RC composite material can be found elsewhere (Kappos 1991, Kwak and Kim 2001).

### 2.1.2. Cyclic envelope

Since a cyclic stress-strain curve describes the changing material properties of concrete under cyclic loadings, its exact definition must be preceded. Nevertheless, unlike the envelope curves obtained from monotonic loading tests, the difficulties in conducting experiments for plain concrete subject to cyclic loadings make it almost impossible to develop a mathematical model of a cyclic

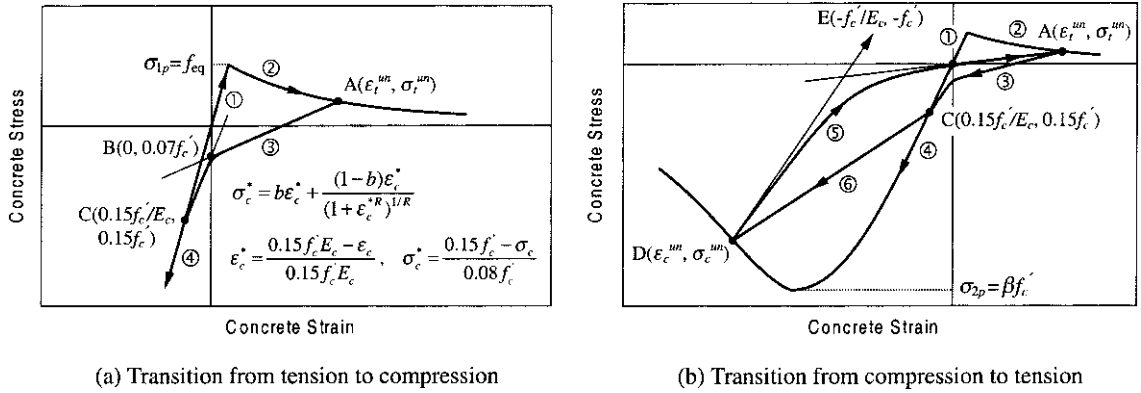


Fig. 3 A proposed cyclic stress-strain relation of concrete

stress-strain curve on the basis of experimental results. The related research has been limited (CEB 1996, Mansour, *et al.* 2001), and only a few simplified cyclic stress-strain curves have been introduced through experimental studies for RC shear panels (Stevens, *et al.* 1991, Mansour, *et al.* 2001). As an example, the simplest cyclic stress-strain curve, which assumes that the unloading-reloading branches always pass the origin regardless of the loading history (Vecchio 1999), is generally used in the nonlinear analysis of RC structures. In addition, linear inelastic unloading-reloading branches have been assumed. These assumptions may lead to a greater difference in structural response between numerical analyses and experimental study as the deformation increases.

To improve the structural behavior of RC shear walls under cyclic loading accompanying large deformation, a curved idealization of unloading-reloading branches in a stress-strain relation is introduced in this paper, on the basis of the steel model used. The proposed cyclic stress-strain relation of concrete is shown in Fig. 3 and can basically be divided into three different regions.

Region 1 (the monotonic envelope curves ①, ②, and ④ in Fig. 3): as mentioned in the monotonic envelope, the monotonic compressive stress-strain curve of concrete is used with the equivalent concrete compressive strength  $\sigma_{2p}$  (see Fig. 3(b)). To describe the biaxial behavior of cracked concrete, which represents a decrease of the compressive strength due to cracks opening after the shear panel cracks, the compressive strength reduction coefficient  $\beta$  in Fig. 3(b) is used (see Eq. (4)). The uniaxial tensile strength of concrete also needs to be reduced to the equivalent tensile strength  $f_{eq}$  as shown in Fig. 3(a) to account for the effect of the compressive stress in the biaxial compression-tension region of the biaxial strength envelope.

Region 2 (the curved regions of ③ and ⑤ in Fig. 3): when unloading is initiated at the tensile stress less than the cracking stress  $f_{eq}$ , the unloading behavior maintains elastic behavior and follows the monotonic envelope curve. Once the cracking stress of concrete is exceeded, however, the unloading behavior follows a different path from the elastic skeleton curve because of microcracks broadly distributed around the cracked region. The experimental results by Stevens, *et al.* (1991) show that the unloading-reloading branches of concrete do not pass through the origin and represent a very soft linear response in the tension region until reaching the zero strain level and an initially stiff response in the compression region (see the branch ③ in Fig. 3(b)). In advance, experimental results (Stevens, *et al.* 1991) also show that the unloading branches originating in the tension region pass the two common points B(0,0.07 $f_c'$ ) and C(0.15 $f_c'/E_c$ , 0.15 $f_c'$ ) in Fig. 3(a) regardless of the position of an unloading point.

Therefore, when the loading is reversed from the tension region to the compression region at point A( $\varepsilon_t^{um}$ ,  $\sigma_t^{um}$ ) in Fig. 3(a), located at the strain softening part, the simplest unloading branch may be defined by a piecewise linear relation connecting the three points of A, B, and C in Fig. 3(a). This simple relation can be effectively used in the case of a small deformation state but may underestimate the energy absorption capacity represented by the area of the stress-strain curve as the deformation increases. Moreover, the hysteretic curve was obtained from the cyclic loading test of concrete panels reinforced with the steel bars. This means that the influence of the steel bars indirectly affects the hysteretic curve. The experimental data representing the relation between concrete stress and corresponding crack width in an uniaxial member subject to cyclic loadings (CEB 1996) also show that the concrete stiffness changes in a gradual manner from zero to almost the maximum initial stiffness when the crack is fully closed, as the crack status changes from opened to closed.

These features make it possible to define the unloading-reloading branches by the following Eq. (5) inferred from the hysteretic curve of steel (Pinto model, Menegotto and Pinto 1973), and its application is limited in the regions from the stress reversal point to the crack closing point (from point A( $\varepsilon_t^{um}$ ,  $\sigma_t^{um}$ ) to point C( $0.15f'_c/E_c$ ,  $0.15f'_c$ ) in Fig. 3(a) and from point D( $\varepsilon_c^{um}$ ,  $\sigma_c^{um}$ ) to point A( $\varepsilon_t^{um}$ ,  $\sigma_t^{um}$ ) in Fig. 3(b)) at which the unloading or reloading curve meets the monotonic envelope curve.

$$\sigma_c^* = b\varepsilon_c^* + \frac{(1-b)\varepsilon_c^*}{(1+\varepsilon_c^{*R})^{1/R}} \quad (5)$$

where  $\varepsilon_c^* = (0.15f'_c/E_c - \varepsilon_c)/0.15f'_c/E_c$ ,  $\sigma_c^* = (0.15f'_c - \sigma_c)/0.08f'_c$  for the unloading branch ③ in Fig. 3.

Eq. (5) represents a curved transition of two straight line asymptotes composed by connecting three boundary points of A( $\varepsilon_t^{um}$ ,  $\sigma_t^{um}$ ), B(0,  $0.07f'_c$ ), and C( $0.15f'_c/E_c$ ,  $0.15f'_c$ ) for the unloading branch ③. For the reloading branch ⑤, a curved transition from a straight line asymptote connecting two points of D( $\varepsilon_c^{um}$ ,  $\sigma_c^{um}$ ) and E( $-f'_c/E_c$ ,  $-f'_c$ ) to another asymptote connecting two points of the origin and point A( $\varepsilon_t^{um}$ ,  $\sigma_t^{um}$ ) at which the unloading was started at the previous loading step. A progressive stiffness degradation according to an increase of deformation, induced by concrete cracking, also has been expressed by Eq. (5) because the straight line asymptotes for the unloading and reloading branches always cross the common points of B(0,  $0.07f'_c$ ) and E( $-f'_c/E_c$ ,  $-f'_c$ ) regardless of the magnitude of deformation, respectively, where the imaginary point E( $-f'_c/E_c$ ,  $-f'_c$ ) is determined from the experimental data by Karsan and Jirsa (1969).

Unlike the steel model where the hardening parameter has a fixed value, the hardening parameter  $b$  in Eq. (5) changes with the loading history. It can be assumed to have a ratio between the slopes of the two straight asymptotes describing the unloading and reloading branches at each load reversal because an already cracked concrete panel cannot sustain the same magnitude of stresses as an uncracked concrete panel due to the presence of open cracks. The points A( $\varepsilon_t^{um}$ ,  $\sigma_t^{um}$ ) and D( $\varepsilon_c^{um}$ ,  $\sigma_c^{um}$ ) will be updated after each stress reversal. On the other hand, the  $R$  value in Eq. (5) cannot be determined easily because the shape of the transition curve depends on many variables affecting to the stress-strain relation of concrete. However, for computational convenience, a constant value of  $R=5$  is assumed in this paper on the basis of correlation studies between numerical results and experimental studies, because it influences the shape of the transition curve even though the  $R$  value itself may have an immaterial effect in the structural behavior of RC panels.

Region 3 (linear region of ⑥ ranging from point C to point D in Fig. 3): the second branch of the unloading curve in the compression region describes the behavior after crack closure up to the maximum compressive strain experienced at the previous loading step. Since relatively large deformation exceeding the peak strain corresponding to the compressive strength occurred, microcracks do not disappear after crack closure and cause the stiffness degradation. That is, a different unloading path from that of the monotonic envelope curve will be followed. The structural behavior in this region represents the proportional increment of the load carrying capacity, and hence the stress-strain curve is assumed with a linear relation.

## 2.2. Steel

### 2.2.1. Monotonic envelope

Reinforcing steel is usually modeled as a linear elastic, linear strain hardening material with yield stress  $f_y$ . However, when reinforcing bars are surrounded by concrete as in membrane elements, the average behavior of the stress-strain relation is quite different, as shown in Fig. 4. The most different feature is the lowering of the yield stress below  $f_y$ .

Yielding of a reinforced concrete panel occurs when the steel stress at the cracked section reaches the yield strength of the bare bar. However, the average steel stress at a cracked element still maintains an elastic stress less than the yield strength because the concrete matrix located between cracks is still partially capable of resisting tensile forces due to the bond between the concrete and reinforcement. Determination of the element stiffness on the basis of the yielding of steel at a cracked section at which a local stress concentration appears in the steel may cause an overestimation of the structural response at the post-yielding range. Since this phenomenon is accelerated with an increase of the deformation, the analysis of RC panels subject to cyclic loadings accompanying relatively large deformations requires the use of average stress-strain relations (Belarbi and Hsu 1994, Stevens, *et al.* 1991).

Accordingly, to trace the cracking behavior of RC panels up to the ultimate limit state by using the smeared crack model in which the local displacement discontinuities at cracks are distributed

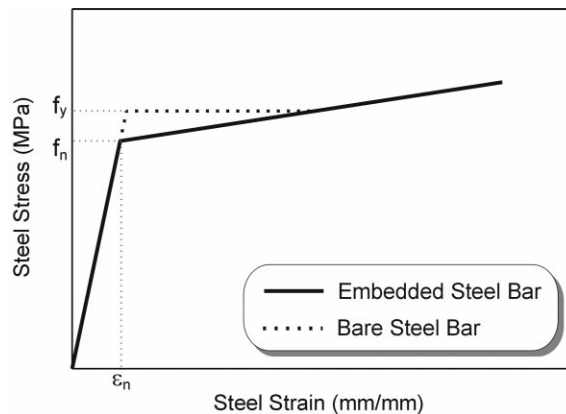


Fig. 4 Average stress-strain relation of steel

over some tributary area within the finite element and the behavior of cracked concrete is represented by average stress-strain relations (Kwak and Song 2002), the average stress-strain relation of steel needs to be defined. Considering these factors, the following linearized average stress-strain relation, which was introduced by Belarbi and Hsu (1994) from the experimental data, is used in this paper to revise the monotonic envelop curve of steel.

$$\sigma_s = E_s \cdot \epsilon_s, \quad \epsilon_s \leq \epsilon_n \tag{6}$$

$$\sigma_s = f_y \left[ (0.91 - 2B) + \left( 0.02 + 0.25B \frac{\epsilon_s}{\epsilon_y} \right) \right], \quad \epsilon_s \geq \epsilon_n \tag{7}$$

where,  $\sigma_s$  and  $\epsilon_s$  represent the average stress and strain respectively, and  $f_y$  and  $\epsilon_y$  are the yield stress and the corresponding yield strain of a bare steel bar. As shown in Eq. (7), the average stress  $\sigma_s$  is a linear function of the parameter  $B=(f'_c/f_y)^{1.5}/\rho$  limited by the boundary strain  $\epsilon_n=\epsilon_y(0.93-2B)$  for the yielding of steel, where  $\rho$  is the percentage of the steel ratio and must be greater than 0.5%. More details for the average stress-strain relation of steel can be found elsewhere (Belarbi and Hsu 1994).

2.2.2. Cyclic envelope

At load reversals, as shown in Fig. 5, the unloading stiffness is assumed to be the same as the initial stiffness. When loading continues in the opposite direction, the stress-strain curve exhibits the Bauschinger effect, which causes nonlinear stress-strain relation and softening of the stress-strain curve before the stress reaches the yield stress in the opposite direction. Among a number of models developed to describe the cyclic stress-strain curve of reinforcing steel (CEB 1996), the most

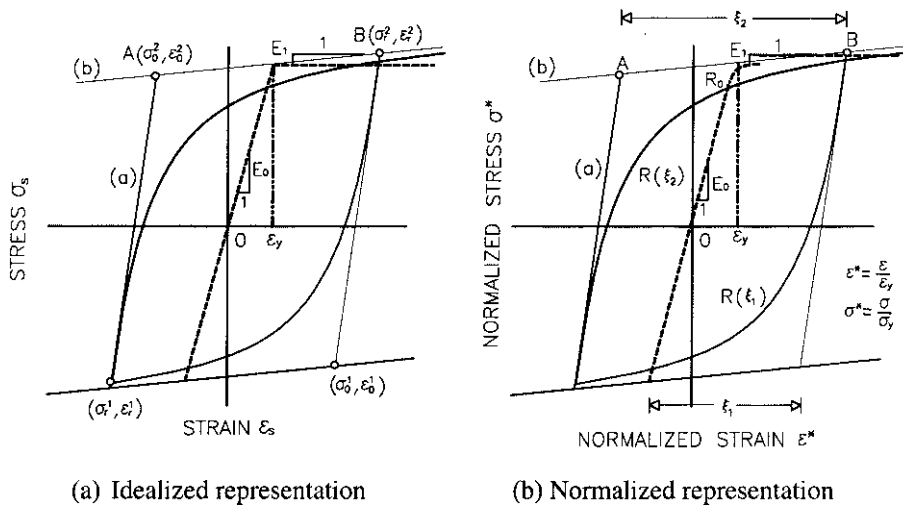


Fig. 5 A hysteretic stress-strain relation of steel

broadly used one is the Giuffr -Menegotto-Pinto (G-M-P) model introduced by Menegotto and Pinto (1973); this model is also adopted in this paper. The stress-strain relation can be expressed by

$$\sigma^* = b\varepsilon^* + \frac{(1-b)\varepsilon^*}{(1+\varepsilon^{*R})^{\frac{1}{R}}} \quad (8)$$

where  $\varepsilon^* = (\varepsilon - \varepsilon_r) / (\varepsilon_0 - \varepsilon_r)$ ,  $\sigma^* = (\sigma - \sigma_r) / (\sigma_0 - \sigma_r)$ . Eq. (8) represents a curved transition from a straight line with slope  $E_0$  to another asymptote with slope  $E_1$  as represented by lines (a) and (b) in Fig. 5. The parameter  $b$  is the strain-hardening ratio between  $E_0$  and  $E_1$ ;  $\varepsilon_0$  and  $\sigma_0$  are the coordinates of the point where the asymptotes of the branch under consideration meet; and  $\varepsilon_r$  and  $\sigma_r$  are the stress and strain of the point where the last strain reversal having stress of the same sign of  $\sigma_0$  took place.  $\varepsilon_0$ ,  $\sigma_0$ ,  $\varepsilon_r$ , and  $\sigma_r$  are updated at each strain reversal.  $R$  is the parameter that controls the shape of the transition curve and allows the representation of the Bauschinger effect. The expression for  $R$  is as follows:

$$R = R_0 - \frac{a_1 \xi}{a_2 + \xi} \quad (9)$$

where  $R$  is a decreasing function of  $\xi$ , which is the strain difference between the current asymptote intersection point  $(\varepsilon_0, \sigma_0)$  and the previous load reversal point with maximum or minimum strain, depending on whether the corresponding steel stress at reversal is positive or negative ( $\varepsilon_r, \sigma_r$ ), as shown in Fig. 5.  $\xi$  is updated following a strain reversal.  $R_0$ ,  $a_1$ , and  $a_2$  are experimentally determined parameters. In this paper, it is assumed that  $R_0=20$ ,  $a_1=18.5$ , and  $a_2=0.15$ .

The original G-M-P model allows a good representation of complete stress-strain cycles but is problematic in terms of representing the isotropic strain hardening effect in the case of partial loading. To improve the applicability of the original G-M-P model, therefore, Filippou, *et al.* (1983) proposed a set of rules to shift the asymptote representing the yielding of steel. By horizontally moving the asymptote by  $\sigma_{st}$  before the asymptote intersection point  $(\sigma_0, \varepsilon_0)$  is newly calculated, the isotropic hardening effect can be considered. The shifting stress  $\sigma_{st}$  is calculated by

$$\frac{\sigma_{st}}{f_y} = a_3 \left( \frac{\varepsilon_{\max}}{\varepsilon_y} - a_4 \right) \quad (10)$$

where  $\varepsilon_{\max}$  is the absolute maximum strain at strain reversal, and  $\varepsilon_y$  and  $f_y$  represent the yielding strain and stress, respectively.  $a_3$  and  $a_4$  are experimentally determined parameters and the same values of  $a_3=0.01$  and  $a_4=7.0$  used by Filippou, *et al.* (1983) are assumed.

As well known through experimental study, for beams with a shorter span or with a higher nominal shearing stress, it takes fewer cycles to reach failure and the recorded load-deflection hysteretic loops exhibit a progressive pinching of loops due to shear deformations (CEB 1996a). This in turn leads to a reduction in the energy absorption capacity of the beam. Roufaiel and Meyer (1987) proposed a modification of the reloading branch in a hysteretic moment-curvature relation on the basis of empirical results to take into account the pinching effect according to the shear span length. Because of its simplicity in application and computational convenience, this model is frequently adopted in the numerical analyses of RC beams.

In the case of RC shear walls, however, the pinching effect due to the shear deformation cannot be implemented into the moment-curvature relation as in a RC beam. When a fixed crack model is adopted to describe the cracking behavior of RC walls, the use of a hysteretic shear stress-slip relation is usually accompanied to reflect the principal strain variation in the principal stress axes. On the other hand, a rotating crack model, which simulates more exact cracking behavior than a fixed crack model, makes it rather difficult to use a hysteretic loop for the shear deformation because the principal axis is assumed to be changed and directed to the maximum principal strain axis normal to the crack surface. In this direction, the relative shear deformation does not appear, meaning that the introduction of a hysteretic loop for shear deformation may be problematic in the case of analyzing RC shear walls using a rotating crack model.

To solve these problems and to consider the shear effect, a direct modification of the stress-strain relation of steel is introduced in this paper. The basic idea was inferred from consideration of shear effect in a RC beam. When a RC wall is subjected to cyclic loading, the unloading and reloading of each material will be repeated according to the loading history. If it is assumed that a reloading starts at point B in Fig. 6 after a few repeated loading cycles, the region between the two boundary points of B and F corresponds to the cracked state of a RC wall accompanying the stiffness degradation due to the bond-slip between the concrete matrix and reinforcing steel; the pinching phenomenon according to the shear deformation will also be concentrated in this region. However, since all the cracks are still open in this region, the shear effect due to the aggregate interlocking seems to be negligibly small. This means that the unloading and reloading behaviors of RC walls accompanying shear effect are wholly governed by the material properties of steel. Upon these considerations, the stress-strain relation of steel is revised in this paper to take into account the shear effect according to the shear span length.

As shown in Fig. 6, after determining a new straight line asymptote connecting two points of  $E(\varepsilon'_0, \sigma'_0)$  and  $A(\varepsilon_1, \sigma_1)$ , instead of the original straight line asymptote connecting two points of  $D(\varepsilon_0, \sigma_0)$  and  $A(\varepsilon_1, \sigma_1)$ , the hysteretic curve of steel, referred to as the “G-M-P model”, can be defined with the two changed straight line asymptotes. That is, the common point where the two

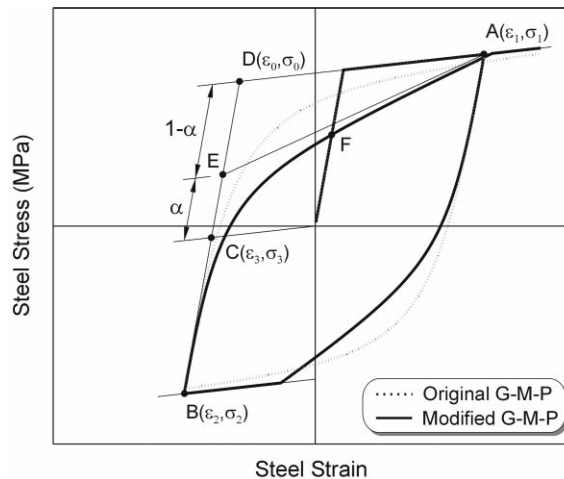


Fig. 6 Stress-strain relation of steel modified for shear effect

asymptotes of the branch under consideration meet is changed from point D( $\varepsilon_0, \sigma_0$ ) to point E( $\varepsilon'_0, \sigma'_0$ ) according to the shear span ratio. Determination of the characteristic point E( $\varepsilon'_0, \sigma'_0$ ) follows the same criteria with those proposed by Roufaiel and Meyer (1987) on the basis of the empirical results.

$$\varepsilon'_0 = \varepsilon_3 + \alpha \cdot \varepsilon_n, \quad \sigma'_0 = \sigma_3 + \alpha \cdot f_n \quad (11)$$

where  $\alpha=0$  for  $h/l < 1.5$ ,  $\alpha=0.4(h/l)-0.6$  for  $1.5 < h/l < 4.0$ ,  $\alpha=1$  for  $h/l > 4.0$ ,  $h$  and  $l$  represent the height and width of the shear wall, and  $(\varepsilon_n, f_n)$  are the average yielding strain and stress in Fig. 4.

### 3. Solution procedure

The reinforced concrete membrane is modeled with a single four-node isoparametric element with

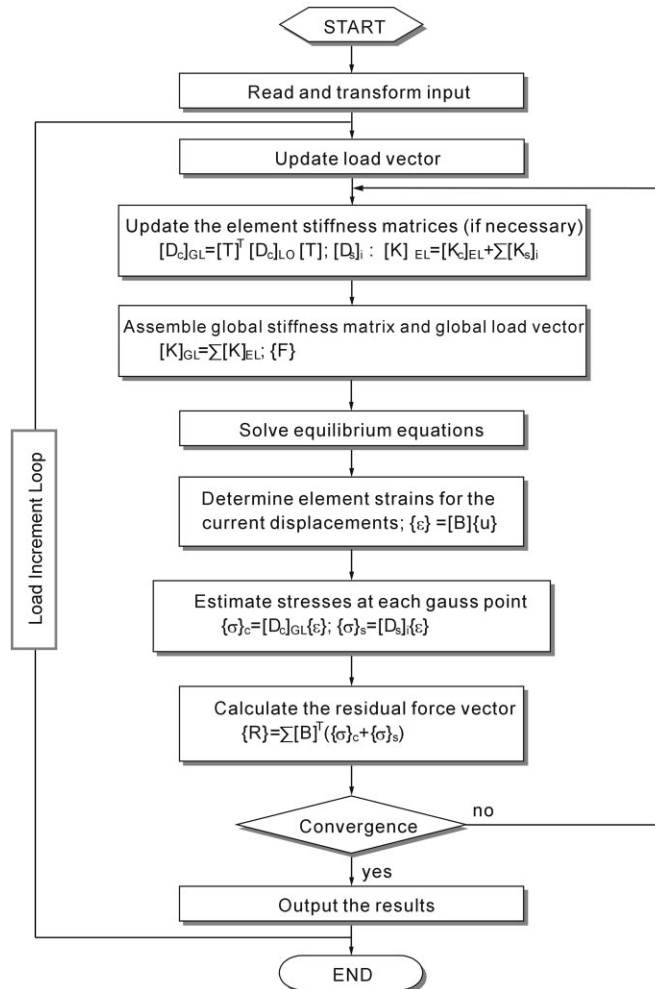


Fig. 7 Solution algorithm for cyclic loading

2 × 2 integration points. A perfect bond between steel and concrete is assumed, and the bond-slip effect is indirectly taken into account through the tension-stiffening model. Considering the nonlinear analysis of structures subject to cyclic loadings by the finite element method, two difficulties arise. The exact prediction of the unloading and reloading points after yielding of steel takes place and the stability of solution procedure are the basic concerns in predicting the hysteretic behavior of a RC structure.

A significant amount of research effort has been concentrated on these issues (CEB 1996, Crisfield 1991), and the arc-length method has recently been adopted as a solution scheme for the material nonlinear analysis of RC structures representing the strength degradation after yielding of steel. By adopting the arc-length method (Crisfield 1991), the complete load-displacement response can be traced including local limit points. As a convergence criterion for the iteration process, the Euclidean norm for displacements was adopted.

$$\|n\| = \sqrt{\{\Delta \mathbf{r}^n\}^T \{\Delta \mathbf{r}^n\}} / \sqrt{\{\mathbf{r}_m\}^T \{\mathbf{r}_m\}} \leq TOL \tag{16}$$

where  $\mathbf{r}_m$  is the nodal displacement vector at the  $m$ -th load step and the convergence tolerance is assumed to be  $TOL=10^{-3}$ . All the remaining procedures, from construction of the element stiffness matrix to the convergence check, follow those used in classical non-linear analysis of RC structures. Fig. 7 shows an outline of the solution algorithm adopted in this paper, and more details for the solution procedure can be found elsewhere (CEB 1996, Crisfield 1991).

### 4. Numerical example

#### 4.1. RC shear panels

##### 4.1.1. Monotonic loading case

The experimental results from reinforced concrete panels tested by Vecchio and Collins (1982) are

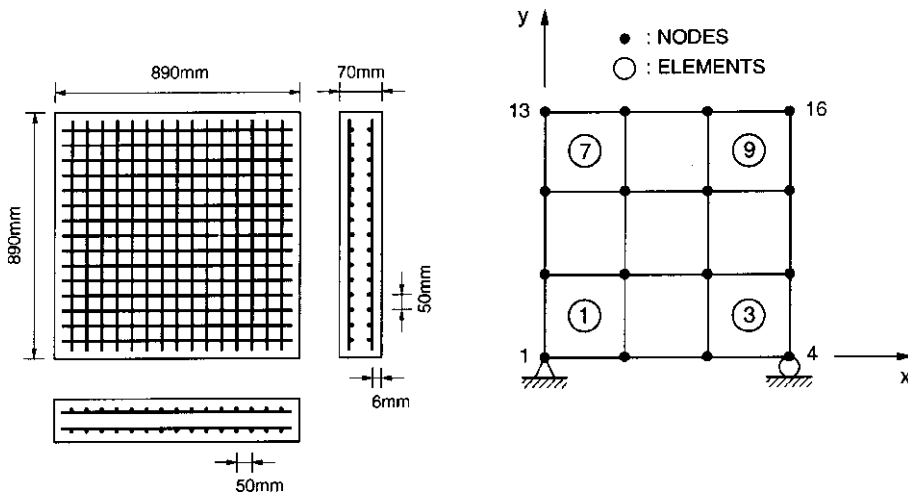


Fig. 8 Configuration and finite element idealization of panel PV series

Table 1 Loading conditions and material properties of shear panels

| Specimen | Loading     |                       | Longitudinal<br>(x direction) |            | Transverse<br>(y direction) |            | Concrete     |          |
|----------|-------------|-----------------------|-------------------------------|------------|-----------------------------|------------|--------------|----------|
|          | $\tau_{xy}$ | $\sigma_x = \sigma_y$ | $\rho_x$                      | $f_{yl}^*$ | $\rho_y$                    | $f_{yt}^*$ | $\epsilon_c$ | $f_c'^*$ |
| PV19     | Monotonic   | 0                     | 0.01785                       | 458        | 0.00710                     | 299        | -0.00215     | -19.0    |
| PV22     | Monotonic   | 0                     | 0.01785                       | 458        | 0.01524                     | 420        | -0.00200     | -19.6    |
| SE8      | Cyclic      | 0                     | 0.02930                       | 492        | 0.00980                     | 479        | -0.00260     | -37.0    |
| SE9      | Cyclic      | 0                     | 0.02930                       | 422        | 0.02930                     | 422        | -0.00265     | -44.2    |

\* unit: MPa

used to validate the analytical models for RC membrane element. These panels were orthogonally reinforced, and had identical dimensions of 890 mm×890 mm×70 mm. The panels were loaded by monotonically increasing forces applied to shear-keys anchored to the perimeters of the specimens. Fig. 8 shows the configuration of the test specimen and the finite element grid used. The loading conditions and the material properties of the panels analyzed herein are given in Table 1, and other assumed material properties were as follows: Poisson's ratio  $\nu=0.2$ , the tensile strength of concrete,  $f_t' = 0.33 \cdot (f_c')^{1/2}$  MPa, and the elastic modulus of steel  $E_{s1}=200,000$  MPa,  $E_{s2}=0.01E_{s1}$  in Fig. 4.

Results of the analyses are compared with the test results in Figs. 9 and 10. Each figure is

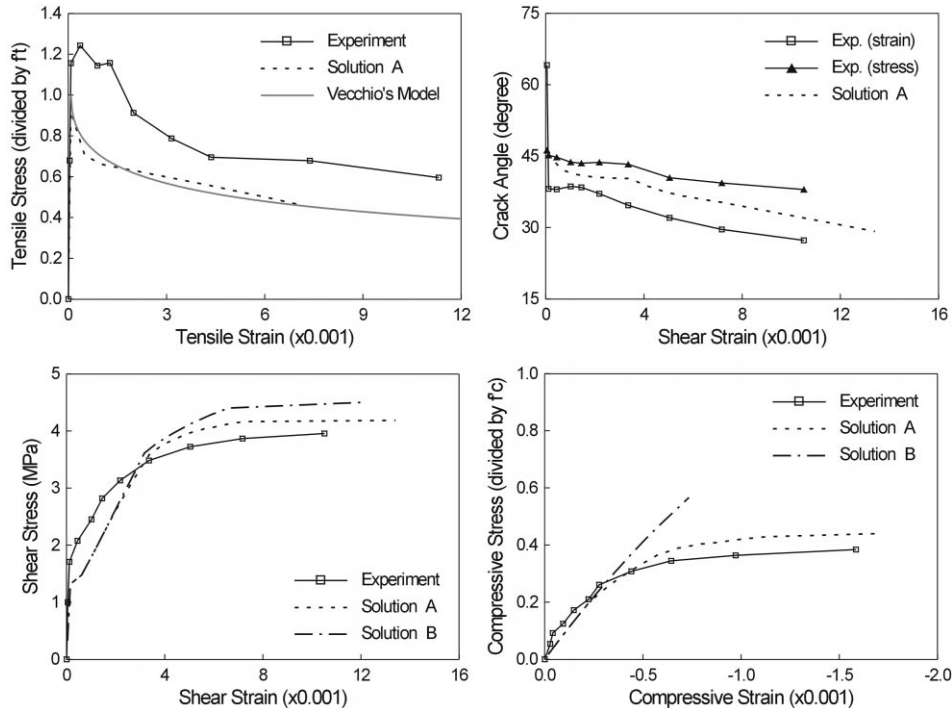


Fig. 9 Comparison of test results and analytical predictions for panel PV19; Solution A: With reduction of compressive strength, Solution B: Without reduction of compressive strength

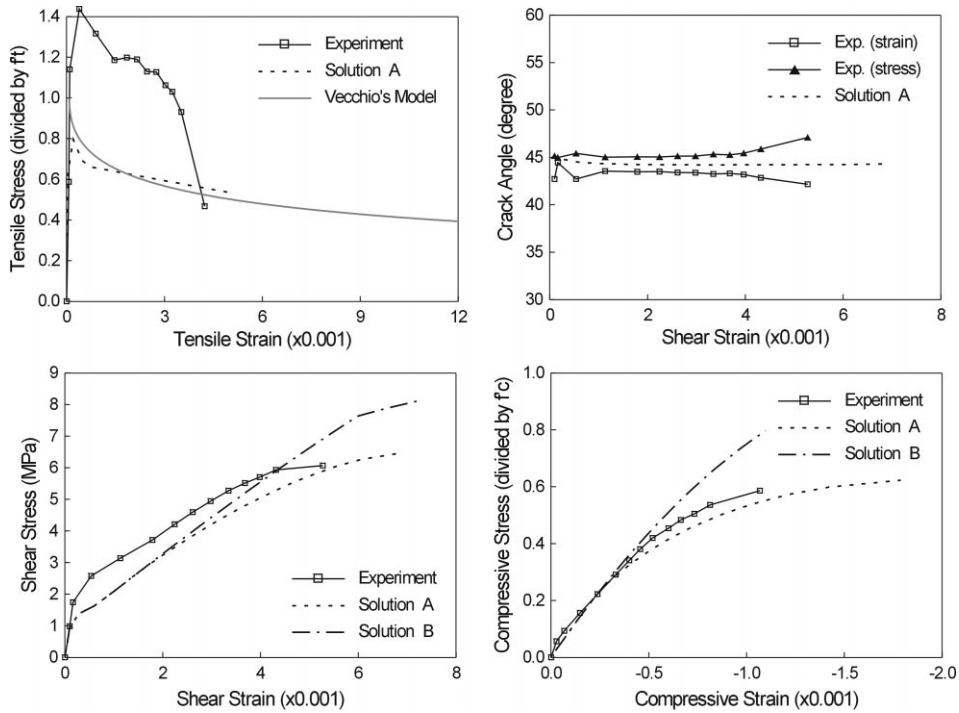


Fig. 10 Comparison of test results and analytical predictions for panel PV22; Solution A: with reduction of compressive strength, Solution B: without reduction of compressive strength

composed of four results representing the relations of principal tensile stress versus principal tensile strain with that of Vecchio's model curve, the orientations of principal stress and strain axes versus shear strain, shear stress versus shear strain, and principal compressive stress versus principal compressive strain with and without reduction of compressive strength.

Panel PV19 in Fig. 9 is a typical specimen having a large difference in the amount of steel in the two directions, causing the collapse mode of concrete shear failure after the yielding of one reinforcement layer. The predicted angle in this study is maintained between the two experimental values, namely, the change in the direction of the principal strains and that of the principal stresses. Since the analysis without reduction of compressive strength leads the panel to failure by the yielding of both reinforcement layers before concrete crushing, this analytical result gives a slight overestimation of ultimate shear capacity and incorrect failure mode.

The calculated response of panel PV22 involves little change in the direction of the principal strains because this panel was heavily and identically reinforced in both directions. As shown in Fig. 10, the analytical solution without reduction of compressive strength indicates that failure is associated with the yielding of both sets of reinforcement, while the experimental results and the analytical solution with compression softening involve concrete shear failure prior to any steel yielding. Accordingly, the analysis without consideration of the compressive strength reduction significantly overestimates the ultimate load capacity.

Based on the rotating crack model, consideration of both tension stiffening and compressive strength reduction gives enhanced analytical results close to the real solution. In addition, for panels

whose load capacities are governed by crushing of concrete, reduction of compressive strength due to tensile cracking should be considered.

#### 4.1.2. Cyclic loading case

In order to establish the applicability of the proposed hysteretic curves, two RC shear panels subject to pure shearing stress are investigated and discussed. Among many experimental results available in the related literature, these two RC panels tested by Stevens, *et al.* (1991) represent typical structural behaviors according to various effects in the stress-strain relation of each material when a severe lateral load such as a seismic load or wind load acts on a shear wall structure. The geometry and cross-section dimensions of the test specimens are presented in Fig. 11(a). Since the same stress state appears over the entire region in an element, only one element is used to trace the structural response according to the loading history (see Fig. 11(b)). The material properties of concrete and reinforcing steel in the panels are given in Table 1, and other assumed material properties not mentioned are the same with those used in the monotonic loading case.

Results of the analyses are compared with the experimental results in Figs. 12 and 13. Since the specimen SE8 is subjected to shear failure after yielding of reinforcing steel in the transverse direction, the experimental result in Fig. 12 shows the yielding behavior of reinforcing steel and represents the ultimate shear resistance converged to about 6 MPa. Hence the structural behavior is directly affected by the yielding strength of steel. Fig. 12(a) shows an analytical result obtained when the stress-strain relation of steel defined in Eqs. (2) and (3) is used; Fig. 12(b) illustrates when the original stress-strain relation of bare steel is used without any modification. It is clear from a comparison of these results with the experimental data shown by the solid line that the modification of the yielding strength of steel gives a very satisfactory agreement of the model with real behavior. When the average yielding strength of steel is not used, the ultimate shear resistance of a RC panel

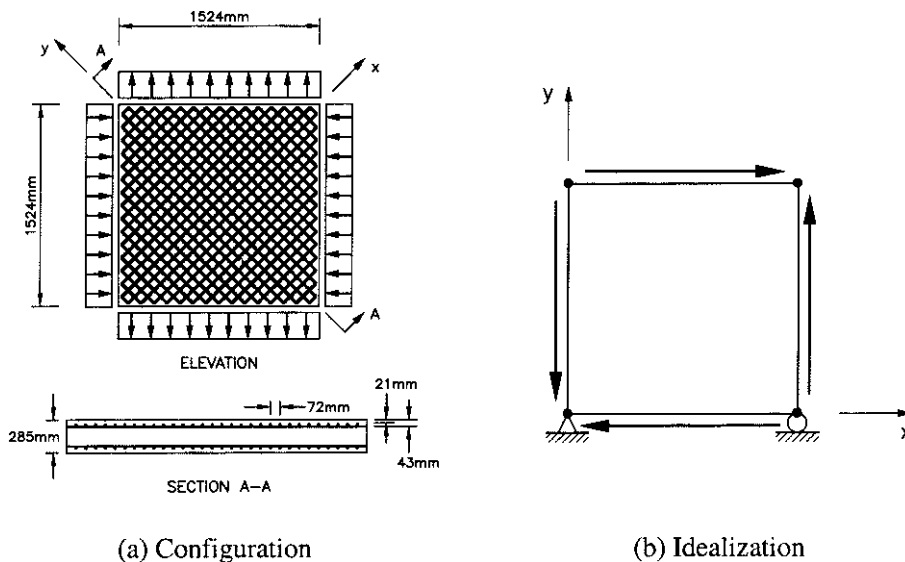


Fig. 11 Configuration and finite element idealization of panel SE series

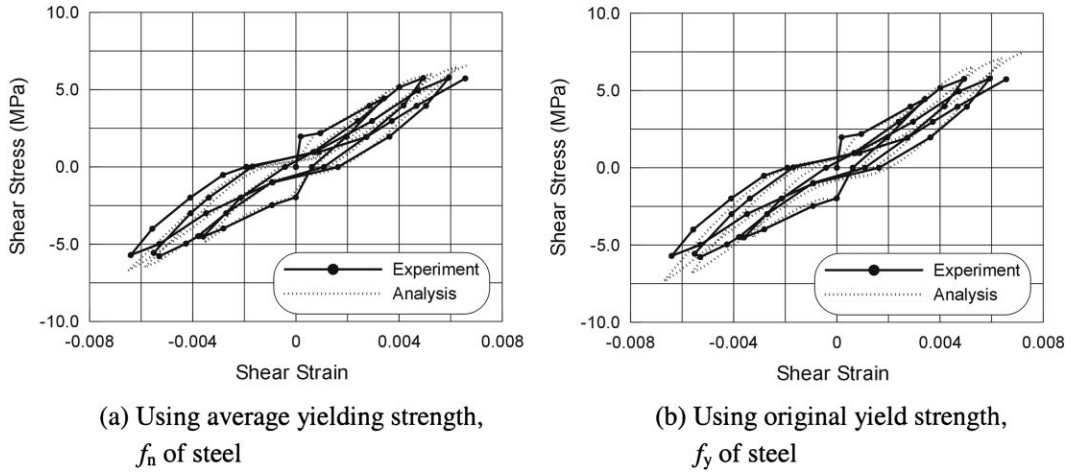


Fig. 12 Shear stress-strain relation for shear panel SE8

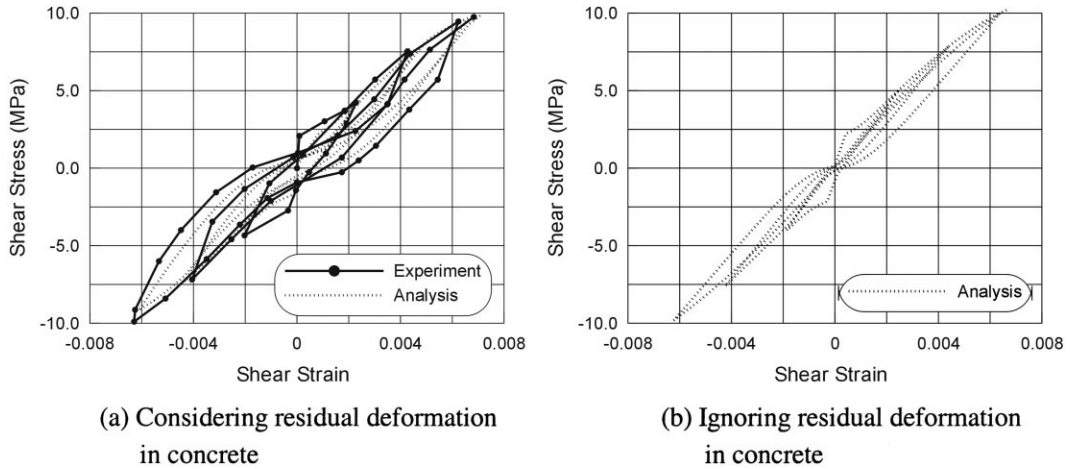


Fig. 13 Shear stress-strain relation for shear panel SE9

subject to cyclic loadings is overestimated, and an incorrect failure mode may result in a RC panel identically reinforced in both directions.

Unlike RC panel SE8, the structural behavior of specimen SE9 is deeply governed by the material property of concrete because of the over-reinforced steel. Fig. 13(a) compares the shear stress-strain relations obtained by the proposed model with the experimental results. Very satisfactory agreement between analysis and experiment is observed. In particular, the pinching phenomenon, caused by the bond-slip between the reinforcing bar and concrete matrix and expressed by the curved unloading and reloading branches with residual deformation in the stress-strain relation of concrete, is effectively simulated in the proposed model, where the residual deformation means the existence of non-zero strains at the zero stresses. This implies that the unloading and reloading branches in the stress-strain relation of concrete do not pass through the origin (see Fig. 3). Otherwise, its exclusion

may lead to an underestimation of the energy absorption capacity of the structure, as shown in Fig. 13(b), and may cause a numerical instability in the analysis of the RC panels as the deformation increases. From Figs. 12 and 13, it is clear that both the effects of the average yielding strength of steel and the residual deformation in concrete must be taken into account to yield a very satisfactory agreement of the numerical model with reality in the case of RC panels subject to cyclic loadings.

## 4.2. RC shear walls

### 4.2.1. Monotonic loading case

The proposed analytical model is also applied to the reinforced concrete shear wall tested by Lefas, *et al.* (1990). Two types of walls were tested: Type I, 750 mm wide  $\times$  750 mm high  $\times$  70 mm thick ( $h/l=1$ ), and Type II, 650 mm wide  $\times$  1300 mm high  $\times$  65 mm thick ( $h/l=2$ ). Among the tested walls, specimens SW13 and SW16 of Type I and specimens SW22, SW24, and SW25 of Type II were analyzed in this study. As shown in Fig. 14, the walls were monolithically connected to an upper and a lower beam. The upper beam provides anchorage for vertical reinforcement and the lower beam provides a rigid base.

Fig. 14 also shows the nominal dimensions of test specimens together with the arrangement of vertical and horizontal reinforcement, deformed steel bars of 8 mm and 6.25 mm diameter, respectively. Additional horizontal reinforcement in the form of stirrups confined the wall edges.

The shear wall specimens were subjected to the combined action of a uniformly distributed axial load and a horizontal load at the upper beam. The axial load remained constant during loading,

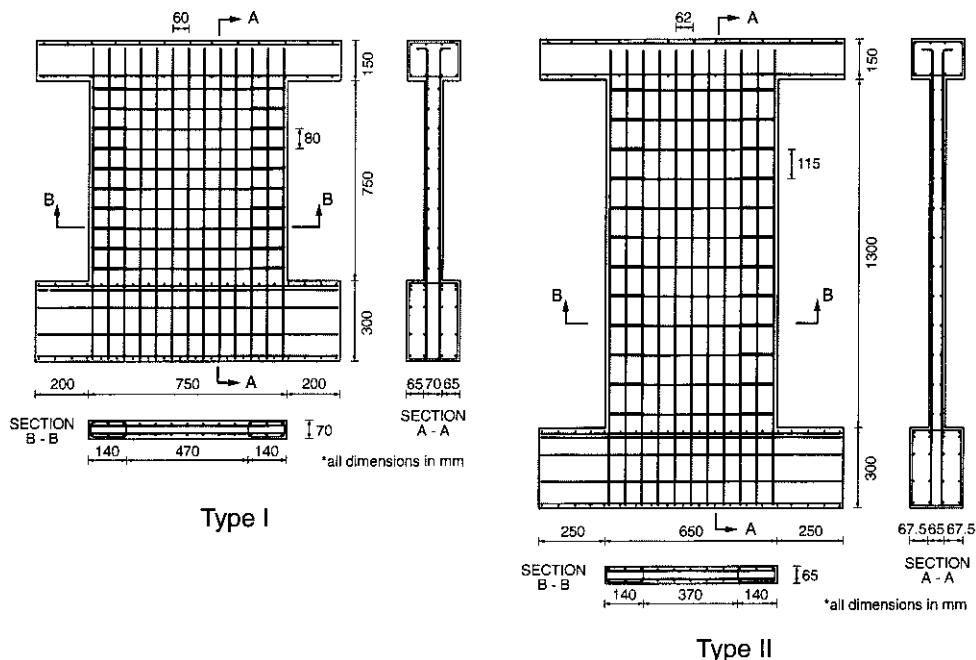


Fig. 14 Geometries and reinforcement details for shear walls

Table 2 Loading conditions and material properties of shear walls

| Wall    | Specimen | Axial load (kN) | $f'_c$ (MPa) | Reinforcement ratios (%) |          |           |          |          |          |          |          |
|---------|----------|-----------------|--------------|--------------------------|----------|-----------|----------|----------|----------|----------|----------|
|         |          |                 |              | Top slab                 |          | Base bock |          | Panel    |          | Ribs     |          |
|         |          |                 |              | $\rho_x$                 | $\rho_y$ | $\rho_x$  | $\rho_y$ | $\rho_x$ | $\rho_y$ | $\rho_x$ | $\rho_y$ |
| Type I  | SW13     | 355             | -34.5        | 0.82                     | 0.97     | 1.68      | 1.05     | 1.10     | 2.40     | 1.55     | 3.10     |
|         | SW16     | 460             | -43.9        |                          |          |           |          |          |          |          |          |
|         | SW22     | 182             | -43.0        |                          |          |           |          |          |          |          |          |
| Type II | SW24     | 0               | -41.1        | 0.82                     | 0.95     | 1.68      | 1.02     | 0.82     | 2.50     | 1.12     | 3.30     |
|         | SW25     | 325             | -38.3        |                          |          |           |          |          |          |          |          |

while the lateral load varied monotonically up to failure. The uniformly distributed gravity load corresponded to 0.1 and 0.2 of the uniaxial compressive strength of the wall cross-section is equal to  $0.85f_{cu}bl$ , where  $f_{cu}$  is the cube strength of concrete,  $b$  is the thickness and  $l$  is the width of the wall. Table 2 includes the material properties and the loading conditions. The material properties not listed in Table 2 are as follows: the uniaxial compressive strength of concrete,  $f'_c=0.85f_{cu}$ ; the tensile strength of concrete,  $f'_t=0.33 \cdot (f'_c)^{1/2}$ ; and the yield strength of the vertical and horizontal reinforcements were 470 MPa and 520 MPa, respectively. All these values except  $f'_t$  are from the experimental data of Lefas and Kosovos (1990).

As shown in Fig. 15, 208 and 320 four-node rectangular elements were used for the analytical discretization of Type I and II specimens, respectively. Fig. 16 shows the analytical load-deflection curves of specimens with the experimental results. As shown in Fig 16, the lateral stiffness and ultimate load capacity of RC shear walls are significantly affected by the level of axial force,

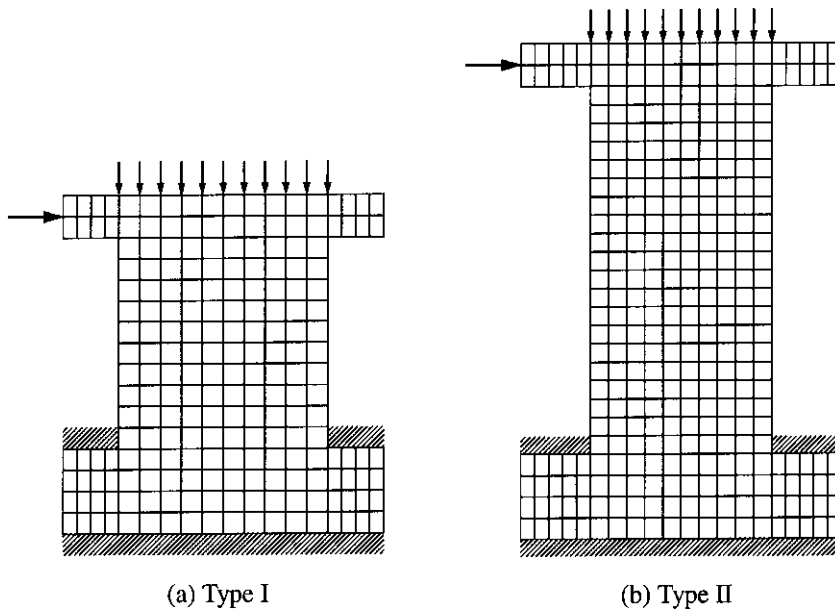


Fig. 15 Finite element mesh configuration used

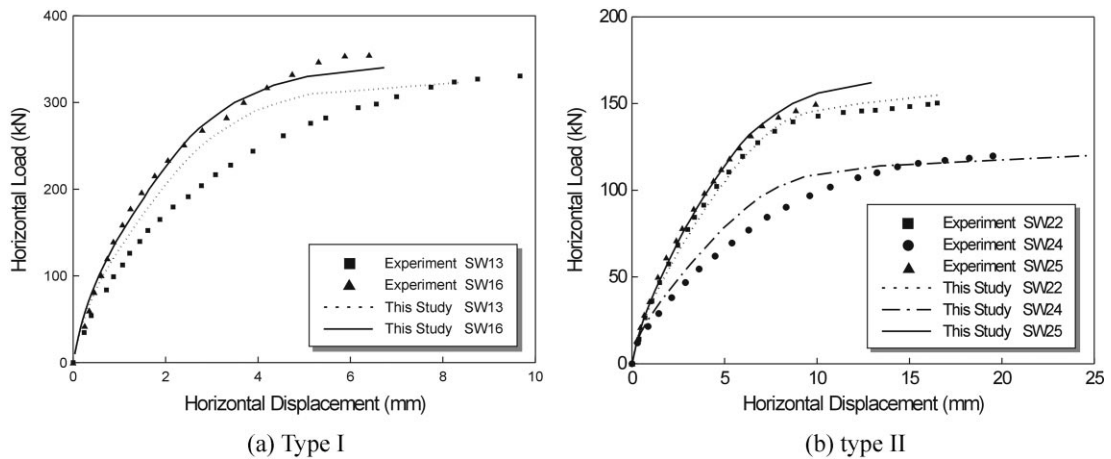


Fig. 16 Comparison of test values and analytical predictions for shear walls

essentially because the applied compressive stress reduces the tensile stress as in a prestressed concrete structure (i.e., the confinement effect). For specimens SW22 and SW25, the predicted load-displacement curves agree very well with the experimental results. The analytical solution of specimen SW25 shows more enhanced ultimate load capacity than that of the experiment. This is because of the premature experimental failure of specimen SW25. For specimen SW24, the analysis underestimates deflections at the beginning of the loading due to a highly evaluated bond effect.

#### 4.2.2. Cyclic loading case

The proposed analytical model is also applied to the reinforced concrete wall B1 tested at the Portland Cement Association (Oesterle, *et al.* 1976). Wall dimensions are shown in Fig. 17, and the material properties and the reinforcement ratio are listed in Table 3. In advance, the finite element idealization of the wall is also shown in Fig. 18. The structure is modeled with 96 four-node elements, and nodes at the base of the wall are fully restrained against horizontal and vertical translations. The top slab is considered to be rigid to distribute the load to the entire cross section. The cyclic loadings applied are assumed to act at the center point in terms of the transverse displacements increased or decreased by 25 mm at each load level, and displacements with the same magnitude are applied three times repeatedly at each load level.

Figs. 19(a) to 19(c) show the experimental and the analytical load-deflection relations. This wall was analytically studied previously by Sittipunt and Wood (1995) (see Fig. 19(d)). The experimental load-deflection relations show pinched hysteretic loops indicating shear dominant behavior. This is primarily because the shear behavior of a RC structure is mainly governed by the bond-slip between the concrete matrix and reinforcing bar. In advance, the numerical results in Fig. 19(b), which are obtained by considering the shear effect through the modification of the stress-strain relation of steel, show an excellent agreement with experimental results through the entire response. The numerical model introduced in this paper gives more improved numerical results than those obtained with the previous numerical models.

If the shear effect is not taken into account in the numerical model, however, there is a marked

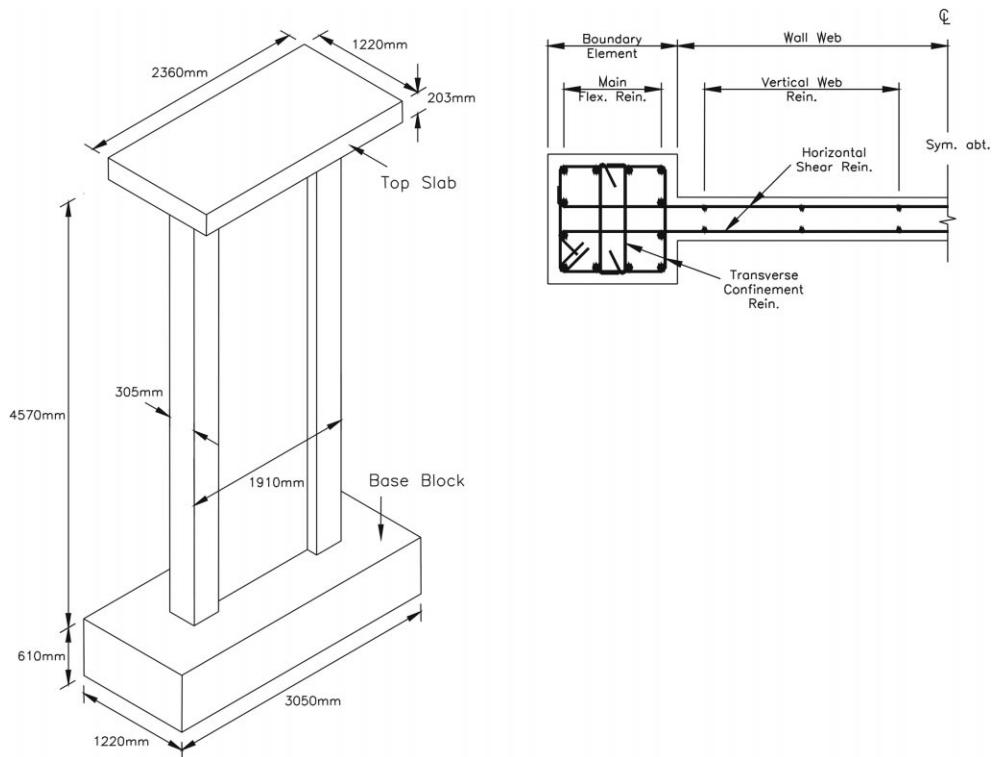


Fig. 17 Details of wall B1

Table 3 Material properties for wall B1

| Properties                         | Wall B1          |       |
|------------------------------------|------------------|-------|
| Cross section shape                | Barbell          |       |
| $f_c'$ (MPa)                       | 53.0             |       |
| Yield strength,<br>$f_y$ (MPa)     | Boundary element | 449.5 |
|                                    | Vertical web     | 520.6 |
|                                    | Horizontal web   | 520.6 |
| Reinforcement ratio,<br>$\rho$ (%) | Boundary element | 1.11  |
|                                    | Vertical web     | 0.29  |
|                                    | Horizontal web   | 0.31  |

difference between the analytical results and the experimental results, and this difference will be larger as the deformation increases. Fig. 19(c) illustrates the influences of the shear effect on the structural behavior. The numerical results ignoring the shear effect represent an overestimated energy absorption capacity and indirectly illustrate why the previous numerical models, which cannot consider the shear effect, may have some difficulties in the modeling of RC walls dominantly affected by the shear force.

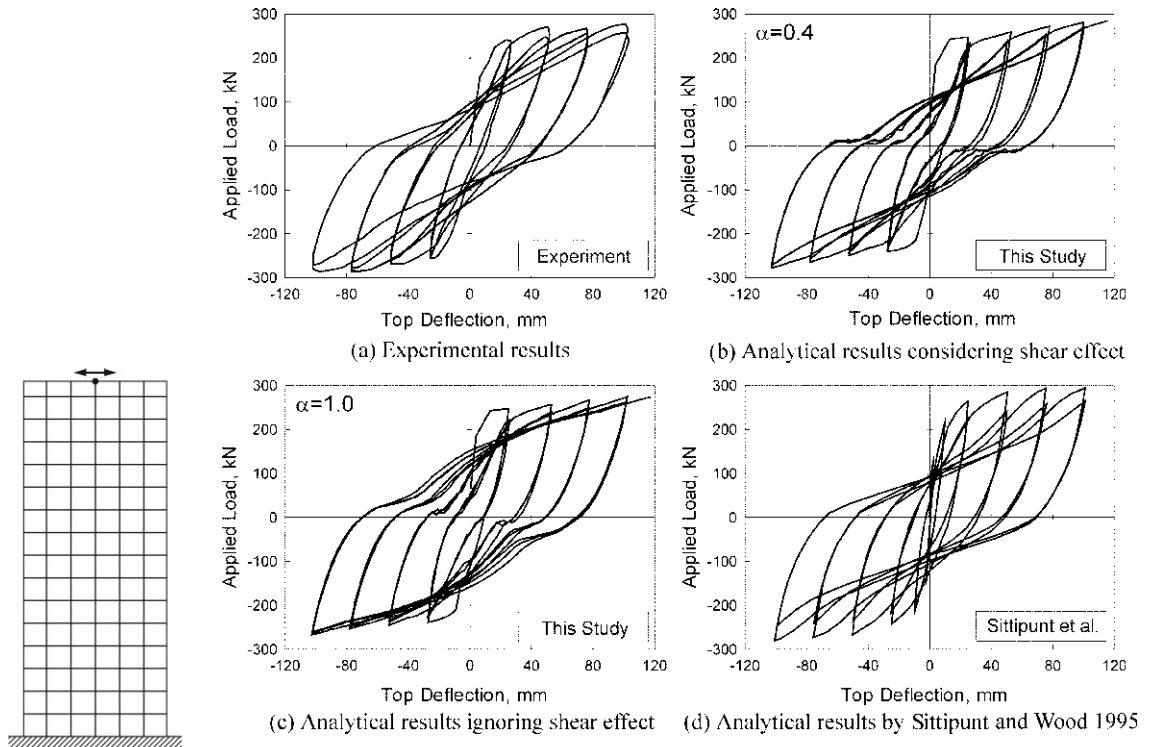


Fig. 18 Finite element idealization of wall B1

Fig. 19 Load-deflection relations of wall B1

## 5. Conclusions

A constitutive model for the analysis of reinforced concrete shear walls subject to general reversed cyclic loadings is introduced. This model describes the most representative characteristic features on the effect of cyclic shear. With adoption of the rotating crack approach, which can effectively describe the concrete cracking under cyclic loadings, simple hysteretic rules defining the cyclic stress-strain relations of concrete and steel are designed on the basis of the theoretical background for the shear dominant structural behavior.

In contrast to a linearized simple hysteretic stress-strain curve of concrete, the use of curved unloading and reloading branches inferred from the stress-strain relation of steel considering the Bauschinger effect gives more improved structural responses. A modification of the stress-strain relation of steel is also introduced to take into account the stiffness degradation and pinching effect on the basis of the criteria adopted in the moment-curvature relation of a RC beam.

## Acknowledgements

The research reported in this paper was made possible by the financial support from the Smart Infra-Structure Technology Center funded by the Korea Science and Engineering Foundation. The

authors would like to express their gratitude to this organization for the financial support.

## References

- Belarbi, A. and Hsu, T.T.C. (1994), "Constitutive laws of concrete in tension and reinforcing bars stiffened by concrete", *ACI Struct. J.*, **91**, 465-474.
- CEB. (1996), "RC elements under cyclic loading: state of the art report", London: Thomas Telford Services Ltd..
- CEB. (1996a), "RC frames under earthquake loading: state of the art report", London: Thomas Telford Services Ltd..
- Crisfield, M.A. (1991), *Non-linear Finite Element Analysis of Solids and Structures*, Vol. 1: Essentials. John Wiley & Sons, Chichester.
- Filippou, F.C., Popov, E.P. and Bertero, V.V. (1983), "Effects of bond deterioration on hysteretic behavior of reinforced concrete joints", Berkeley: Earthquake Engineering Research Center, Univ. of California, EERC 83-19.
- Kappos, A.J. (1991), "Analytical prediction of the collapse earthquake for R/C buildings: suggested methodology", *Earthquake Engineering and Structural Dynamics*, **20**, 167-176.
- Karsan, I.D. and Jirsa, J.O. (1969), "Behavior of concrete under compressive loading", *J. Struct. Div., ASCE*, **95**, 2543-2563.
- Kupfer, H.B. and Gerstle, K.H. (1973), "Behavior of concrete under biaxial stresses", *J. Eng. Mech. Div., ASCE*, **99**, 852-866.
- Kwak, H.G. and Kim, D.Y. (2001), "Nonlinear analysis of RC shear walls considering tension-stiffening effect", *Computers and Structures*, **79**, 499-517.
- Kwak, H.G. and Song, J.Y. (2002), "Cracking analysis of RC members using polynomial strain distribution function", *Eng. Struct.*, **24**, 455-468.
- Lefas, L.D., Kosovos, M.D. and Ambraseys, N.N. (1990), "Behavior of reinforced concrete structural walls: strength, deformation characteristics, and failure mechanism", *ACI Struct. J.*, **87**, 23-31.
- Mansour, M., Lee, J.Y. and Hsu, T.T.C. (2001), "Cyclic stress-strain curves of concrete and steel bars in membrane elements", *J. Struct. Eng., ASCE*, **127**, 1402-1411.
- Menegotto, M. and Pinto, P.E. (1973), Method of analysis for cyclically loaded reinforced concrete plane frames including changes in geometry and nonelastic behavior of elements under combined normal force and bending. In: *IABSE, Proceedings of IABSE Symposium on Resistance and Ultimate Deformability of Structures Acted on by Well Defined Repeated Loads*, Lisbon, Spain.
- Oesterle, R.G., Fiorato, A.E., Johal, L.S., Carpenter, J.E., Russell, H.G. and Corley, W.G. (1976), Earthquake resistance structural walls-tests of isolated walls. Skokie, Illinois: Construction Technology Laboratories, Portland Cement Association, p.315.
- Penelis, G.G. and Kappos, A.J. (1997), "Earthquake-resistant concrete structures", London: E & FN SPON.
- Roufaiel, M.S.L. and Meyer, C. (1987), "Analytical modeling of hysteretic behavior of R/C frames", *J. Struct. Eng., ASCE*, **113**, 429-444.
- Sittipunt, C and Wood, S.L. (1995), "Influence of web reinforcement on the cyclic response of structural walls", *ACI Struct. J.*, **92**, 745-756.
- Stevens, N.J., Uzumeri, S.M. and Collins, M.P. (1991), "Reinforced concrete subjected to reversed cyclic shear-experiments and constitutive model", *ACI Struct. J.*, **88**, 135-146.
- Stevens, N.J., Uzumeri, S.M., Collins, M.P. and Will, G.T. (1991), "Constitutive model for reinforced concrete finite element analysis", *ACI Struct. J.*, **88**, 49-59.
- Vecchio, F.J. and Collins, M.P. (1982), "The response of reinforced concrete to in-plane shear and normal stress", Toronto: Dept. of Civil Eng., Univ. of Toronto, Publication No. 82-03.
- Vecchio, F.J. and Collins, M.P. (1993), "Compression response of cracked reinforced concrete", *J. Struct. Eng., ASCE*, **119**, 3590-3610.
- Vecchio, F.J. (1999), "Towards cyclic load modeling of reinforced concrete", *ACI Struct. J.*, **96**, 193-202.